Properties of mid-latitude cirrus cloud from surface Ka-band radar observations during 2014-2017

Juan Huo, Yufang Tian, Xue Wu, Congzheng Han, Bo Liu, Yongheng Bi, Shu Duan and Daren Lu

Key Laboratory for Atmosphere and Global Environment Observation, Chinese Academy of Sciences

5   *Correspondence to*: Juan Huo (huojuan@iap.ac.cn)

Abstract. The physical properties and radiative role of cirrus clouds remain one of the uncertainties in the Earth–atmosphere system. In this study, we present a detailed analysis of cirrus properties based on four years of surface millimetre wavelength radar measurements in Beijing, China, where summer monsoon from the ocean and winter monsoon from the continent prevails alternately, resulting in various cirrus clouds. More than 6600 cirrus clusters were studied to quantify the properties of

10   cirrus clouds, such as the height, optical depth and horizontal extent, which can serve as a reference for parameterization and characterization in global climate models. In addition, comparison between cirrus clusters formed under summer monsoon and winter monsoon indicates the different formation and evolution mechanisms of cirrus. Statistically, the temperature of more than 90% of cirrus bins are below −15ºC. The dependence of the radar reflectivity of cirrus particles on the height and temperature was also observed in this study, indicating that the reflectivity of cirrus bins increases (decreases) as the

15   temperature (height) increases. In addition, it was found that there is a strong linear relationship between the mean reflectivity and the cirrus cloud depth. Due to various synoptic circumstances, the cirrus clouds in summer are warmer, higher, and thicker, with larger reflectivity than that in winter; in particular, the mean cloud-top height of cirrus clouds in summer is 2.5 km higher than that in winter. It was found that most cirrus clusters in winter are likely to be the in situ origin type cirrus but some cirrus clusters in summer are the in situ origin cirrus and others are the liquid origin type cirrus.

20   ## 1.   Introduction

According to the definition from the Glossary of the American Meteorological Society (AMS, 2019), the primary cirrus cloud types are cirrus, cirrostratus, and cirrocumulus, and the term "cirrus cloud" is frequently used for all types of cirriform clouds. Cirrus clouds are detached cirriform elements in the form of white, delicate filaments, of white (or mostly white) patches, or of narrow bands, that are composed of ice crystals. Cirrus clouds absorb the outgoing infrared radiation from Earth's surface and

25   lower atmosphere while reflecting a portion of the incident sunlight back to outer space. When cirrus clouds are thin enough that the sun can be seen through them, the net impact on the planetary radiation balance is generally one of warming; thicker cirrus reflect more sunlight and generally result in net cooling (Heymsfield et al. 2017; Kärcher 2018; Kox et al. 2014). Among all cloud types, only cirrus clouds exert potential warming effects on the Earth–atmosphere energy system. Studies show that the occurrence frequency of cirrus clouds exhibits latitudinal variability ranging from 50% in the equatorial regions of Africa

30   to 7% in the polar regions (Hahn and Warren 2007; Sassen et al. 2008, 2009; Stubenrauch et al. 2006). Cirrus clouds are an important component of the planetary radiation budget in terms of magnitude; plus, they influence hydrological and climate sensitivities and affect surface climate (Lawson et al. 2019; Yang et al. 2015).

The physical and optical properties of cirrus clouds, such as ice crystal size, ice shape, particle concentration, cloud-top height, and optical depth, are heterogeneously and diversely distributed over the globe (Adhikari et al. 2012; Cotton et al. 2013;
35   Ge et al. 2019; Heymsfield et al. 2013; Jensen et al. 1996; Luebke et al. 2016; Mace et al. 2006; Yang and Fu 2009). Recent studies show that cirrus clouds remain one of the largest uncertainty sources in global climate models (GCMs), due to the deficiencies in representing their observed spatial and temporal variability (Joos et al. 2014; Muhlbauer et al. 2014; Zelinka et al. 2012). According to the IPCC (Boucher et al. 2013), "Especially for ice clouds, and for interactions between aerosols and clouds, our understanding of the basic micro-scale physics is not yet adequate, although it is improving." Understanding the
40   microphysical and macrophysical properties of cirrus clouds, as well as their relationships with atmospheric states, such as temperature, wind velocity and relative humidity, is important for advancing our fundamental understanding of the formation and life cycles of cirrus cloud. It is also an essential step toward reducing the uncertainties of estimates of the climatic impact of cirrus and improving the representation of cirrus clouds in GCMs.

Millimetre wavelength radar is a powerful method for observing the macroscopic and microphysical properties of cloud
45   vertical profiles owing to its ability to penetrate the interior of clouds. Because of their short wavelengths, they are sensitive to small cloud droplets and ice crystals, meaning they detect all types of non-precipitating clouds well (Kollias et al. 2007). This study used long-term continuous surface Ka-band radar data to study and understand the microphysical and macrophysical properties of cirrus clouds over Beijing, China, in the northern mid-latitude region. Beijing (39.96°N, 116.37°E) is in the subtropical monsoon zone with a typical continental monsoon climate. Winds from southeast ocean prevail in summer while
50   winds from northwest continent dominate in winter, resulting in hot and rainy summers but cold and dry winters. The formation, evolution and life cycle of cirrus clouds present regional and distinctive traits, which are created by the regional climate and, to a certain extent, the global climate too. This paper presents the features of cirrus clouds over mid-latitude monsoon regions through detailed analysis based on long-term radar data, and serves as a reference for cloud parameterization in GCMs.

55   Section 2 of this paper briefly introduces the Ka-band radar data, the identification method for cirrus clouds, and other auxiliary datasets. Section 3 describes the macrophysical properties of cirrus clouds. Details of the microphysical properties of cirrus clouds are presented in section 4. In section 5, the formation types of cirrus in winter and summer are investigated. Conclusions are given in section 6.

2. Cirrus observation and identification by Ka-band radar

2.1 Ka-band radar

The cirrus clouds analysed in this study are from observations of a Ka-band polarization Doppler radar (KPDR) situated at the Institute of Atmospheric Physics (IAP, 39.967°N, 116.367°E), Beijing, China. KPDR was set up in 2010 and works at a frequency of 35.075 GHz (wavelength of 8.55 mm) (Huo et al. 2019), measuring the reflectivity, Doppler velocity, spectral width and linear depolarization ratio of cloud. It is equipped with a Magnetron-type transmitter using a reflectivity factor threshold of −45 dBZ for cloud determination, which has stronger detection capability than the Ka-band radar with all-solid type transmitter. The pulse width is 0.2 μs and the beam width is 0.4°. Its repetition frequency is 3.5 KHz and its vertical resolution is 30 m. KPDR has operated daily since 2012, mostly in the vertically pointing mode. During special events—for example, short-term collaborative observations with other instruments—the scanning mode changes to the Plane Position Indicator or Radar Height Indicator mode. In 2013 and 2018, KPDR was non-operational during almost the whole of the summer period. The radar data used in this paper were observed from 1 January 2014 to 31 September 2017. During these four years, the valid operational time of the radar in the vertically pointing mode occupied more than 80% of the total time. It should be noted that KPDR is insensitive to very small particles and it is possible that KPDR will miss some clouds with reflectivity out range of the detection threshold. The missed percentage is inaccessible at present due to our incomplete understanding of cirrus clouds and limitations of observation condition; however, it should be small according to the radar capability.

2.2. Cirrus identification

As stated in the introduction, the Glossary of the American Meteorological Society (AMS, 2019) describes and defines cirrus cloud primarily from its appearance. However, such a definition is not applicable for the cloud classification of the KPDR data, especially those observed with a small field of few (FOV) in the vertically pointing mode. Sassen et al. (2008) classified cloud layers as cirrus via defining two criteria; namely, the visible optical depth should be less than 3.0 and the cloud-top temperature should be lower than –40 °C, categorizing cirrus clouds via cloud physical and optical parameters. Heymsfield et al. (2017) indicated that cirrus clouds form primarily in the upper troposphere, above about 8 km, where temperatures are generally below −30°C. In the cloud classification algorithm developed for the Cloud Profiling Radar onboard the CloudSat satellite, the average temperature at the largest radar equivalent reflectivity factor (Ze), the average largest Ze, the average height of the maximum Ze, the cloud-base height, etc., are combined to determine cirrus cloud (Wang and Sassen 2001b). Ge et al. (2019) used two temperature criteria to identify cirrus cloud: the temperature of the cloud top should be less than −30°C and the temperature at the maximum Ze layer and at the cloud base should be less than 0°C.

KPDR has a cloud clustering and classification algorithm, a detailed description of which has been presented by Huo et al. (2019). Here, we briefly describe it as follows. The KPDR cloud profiles firstly are grouped as clusters based on a combination of a time–height clustering method and a k-means clustering method. After each cloud cluster is determined, a fuzzy logic method is applied using multiple cloud properties, such as cloud-base height, cloud depth, radar reflectivity, etc., to classify the

cloud cluster into nine types: Cs, Cc, Ac, As, St, Sc, Ns, Cu and Cb clouds. Clouds identified as Cs and Cc are the objects of this study. Further, in order to ensure all cirrus clouds are determined exactly, two criteria have been added after the classification algorithm; namely, the cloud-top temperature should be less than −30°C and the cloud-base temperature should be less than 0°C. In some studies (Krämer et al. 2016; Luebke et al. 2016; Heymsfield et al. 2017; Wolf et al. 2018), cirrus clouds are defined as ice clouds with lower temperature < -38℃. In this study, according to the Glossary of the American Meteorological Society (AMS, 2019), the cirrus clouds are referred to all types of cirriform clouds (Ci, Cc and Cs clouds), which is determined by the reflectivity, temperature, height and depth.

2.3 Other datasets

In this study, we also used some other datasets to complement our investigation of the properties of cirrus cloud, such as the temperature profile, water vapor, wind velocity, cloud optical thickness, etc. The research datasets of cloud optical thickness (produced from Himawari-8) used in this paper were supplied by the P-Tree System, Japan Aerospace Exploration Agency (https://www.eorc.jaxa.jp/ptree/index.html, last access: 6 January 2020). Other meteorological reanalysis data employed were from the European Centre for Medium-Range Weather Forecasts (ECMWF) ERA5 datasets (https://www.ecmwf.int/en/forecasts/datasets/reanalysis-datasets/era5; last access: 6 January 2020).

3. Macrophysical properties of cirrus clouds

3.1 Cirrus cloud samples under summer and winter monsoon

Cirrus clouds can be vertically and horizontally extensive, with their various appearances dependent on the diverse range of associated atmospheric movements and processes. KPDR is located in the north of the North China Plain, where to the west and north are mountains and to the south and east is the Bohai Sea. In the region's hot summers, monsoon from the sea brings large quantities of water vapor, whereas dry and cold monsoon from the northern continent dominates this region in winter. These different monsoon types support various atmospheric conditions, such as increasing relative humidity, cooling, updrafts, etc., required for the formation of cirrus clouds, ultimately resulting in distinct cirrus distributions. Figure 1 presents a typical example of a cirrus cloud distribution collected by KPDR in one month of winter (January 2016) and one month of summer (August 2015).
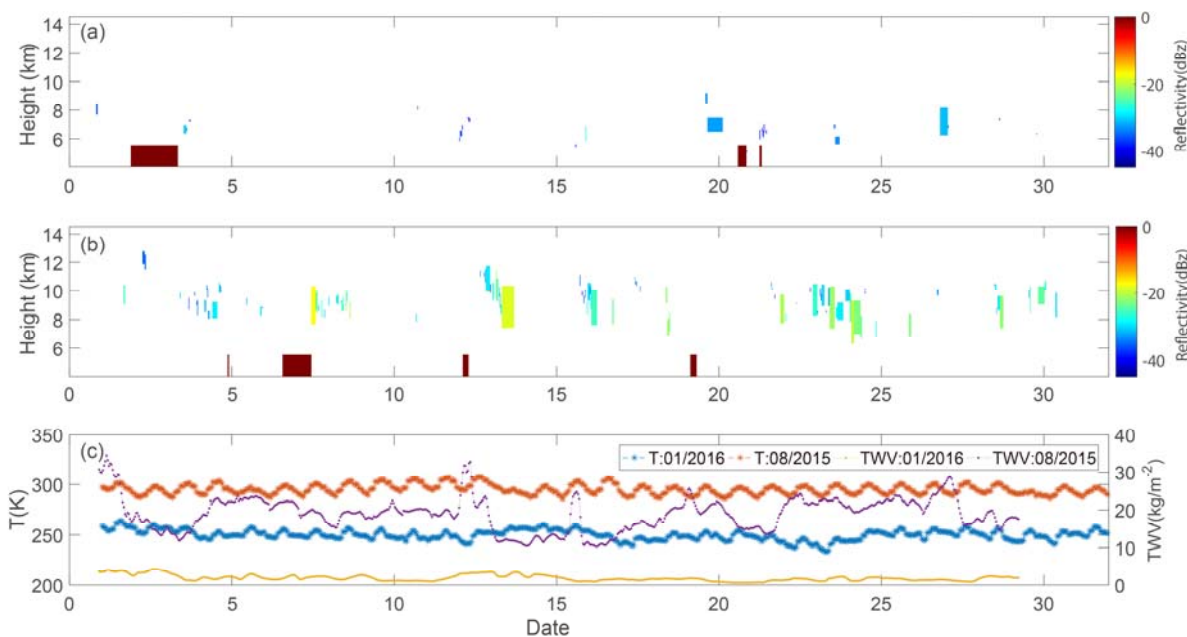
115

Figure 1. Cirrus clouds occurring in (a) January 2016 (winter) and (b) August 2015 (summer). The mean cloud-top height, mean base height and lifetime of each cirrus cluster forms a cirrus "rectangle". Its mean radar reflectivity is illustrated with different colours. Dark red rectangles on the horizontal axis indicate periods without vertically pointing radar measurements. The surface temperature (T, left-hand y-axis) and total water vapor (TWV, right-hand y-axis) in the two months are presented in (c).

There are more cirrus clusters in August than in January, and the mean radar reflectivity of cirrus in August is higher than that in January. Cirrus clouds in August also show larger vertical dimensions than in January. The temperature and amount of water vapor are two key parameters in the formation of clouds, especially in plain areas where orographic uplift is negligible. The strong contrast in the climatic circumstances between a month in summer and a month in winter generates a diverse range of cirrus clouds (Fig. 1c). Thus, to better understand the physical or optical properties of cirrus clouds, statistical analyses were carried out in this study for different seasons. Such comparisons of the cirrus clouds among the four seasons benefit our understanding of the dominant formation origins of cirrus clouds when a region is governed alternately by different monsoon types. In this study, four years of radar observations presented more than 6600 cirrus clusters for our analysis.

3.2 Monthly and hourly occurrence frequency of cirrus clouds

Radar data collected in vertically viewing mode were used to calculate the occurrence frequency of all clouds (O_{all}), which is the ratio of cloudy profiles to all profiles in a certain time range (i.e., an hour or a month), as well as the occurrence frequency of cirrus clouds (O_{ci}), which is the ratio of profiles containing cirrus to all radar profiles:

$$O_{all} = N_{all} / N_r, \qquad (1)$$
$$O_{ci} = N_{ci} / N_r, \qquad (2)$$

135   where N_{all} is the number of cloudy profiles, N_r is the number of all radar profiles, and N_{ci} is the number of cirrus clouds profiles. Figure 2 shows the monthly occurrence frequency of all clouds and cirrus clouds in four years. September has the maximum O_{all} among all months, and summer/winter has the maximum/minimum O_{all} among the four seasons. Relative to O_{all}, O_{ci} decreases to 1/2–1/3, and in winter O_{ci} is about 33% of O_{all}. The average O_{ci} in April and June is about 20%, whereas in winter (December–February) it is no more than 10%. The average O_{ci} in the four years is 16%, which is lower than the cirrus cloud

140   coverage of 24% reported by Hahn and Warren (2007) based on satellite measurements over North China. This might be associated with the observation location and the FOV of the KPDR. Large quantities of water vapor over the sea areas and orographic-lift movements over mountain areas provide advantageous conditions for the formation of clouds, meaning more clouds occur over these areas relative to plain areas. Therefore, the occurrence frequency calculated from the KPDR data with a small FOV are lower than the cloud coverage calculated from data with a broad FOV.
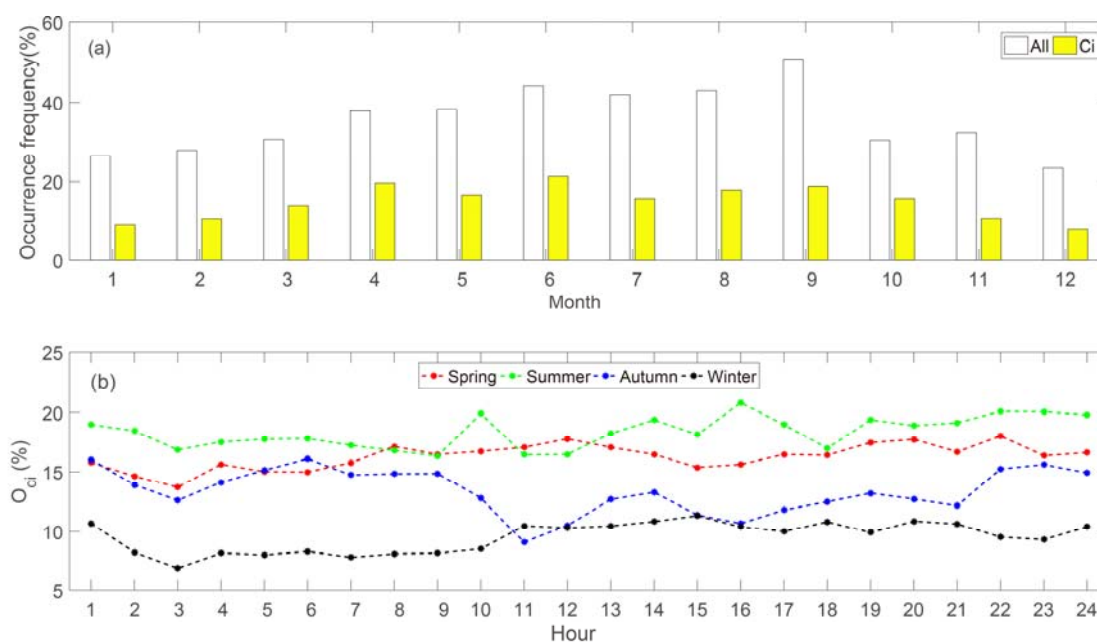
145

Figure 2. Monthly occurrence frequencies of all clouds (O_{all}) and the occurrence frequency of cirrus clouds (O_{ci}) (a) along with the diurnal O_{ci} in the four seasons (b).

KPDR operates continuously and thus allows the diurnal variation of O_{ci} to be studied, which illustrates the potential relationship with local thermal convection caused by solar heating. As shown in Fig. 2a, the three highest O_{ci} values in spring,

150   summer, autumn and winter occur at 22:00/12:00/20:00, 16:00/22:00/23:00, 22:00/23:00/00:00 and 20:00/14:00/00:00,

respectively, indicating larger O_{ci} values appear both at night and during daytime. The hourly variations of O_{ci} in the four seasons are different; however, there is no apparent difference between day and night in each season. The diurnal variation of O_{ci} seems to be insensitive to solar heating, which drives the development of regional thermal convection. Here, the presence of cirrus clouds over KPDR is not closely related with local air-updraft activities, indicating that these cirrus clouds may not be generated locally by thermal convections.

3.3 Height, depth and extent of cirrus clouds

The top height of cirrus clouds indicates the highest condensation level in the troposphere, above which clouds cannot form because of the non-conducive condensation conditions. The base height of cirrus clouds indicates the lowest level required for cirrus formation. In this study, the cloud-top height (CTH) and cloud-base height (CBH) were calculated for each cirrus cloud cluster; specifically, the CTH and CBH are the mean values of all cloudy profiles in a cirrus cluster. The distributions of the mean CTH and CBH of all cirrus clouds in the four seasons are presented in Fig. 3, and Table 1 presents the quantified statistical results.

It is shown that the CTH of cirrus clouds varies in the range of 5.09–13.35 km (Fig. 3a). The difference between the maximum CTH and the minimum CTH is about 7 km in each season, indicating the ranges of the condensation level and various formation mechanisms of cirrus clouds. Besides, differences in the CTH between the four seasons are also apparent. Both the maximum CTH (13.35 km) and the highest mean CTH (10.16 km) are found in summer, whereas winter has the minimum CTH (11.25 km) and lowest mean CTH (7.66 km). In summer, 98% of cirrus clouds have a CTH greater than 8 km and 57% are greater than 10 km. In winter, only 37% of cirrus clouds have a CTH larger than 8 km, and those with a CTH higher than 6 km account for 94%. The mean CTH in summer is 2.5 km higher than that in winter, which means the average condensation level in summer is also 2.5 km higher. Spring and autumn are two transition seasons and their CTHs are 8.95 km and 9.09 km, respectively, which are between those of summer and winter.
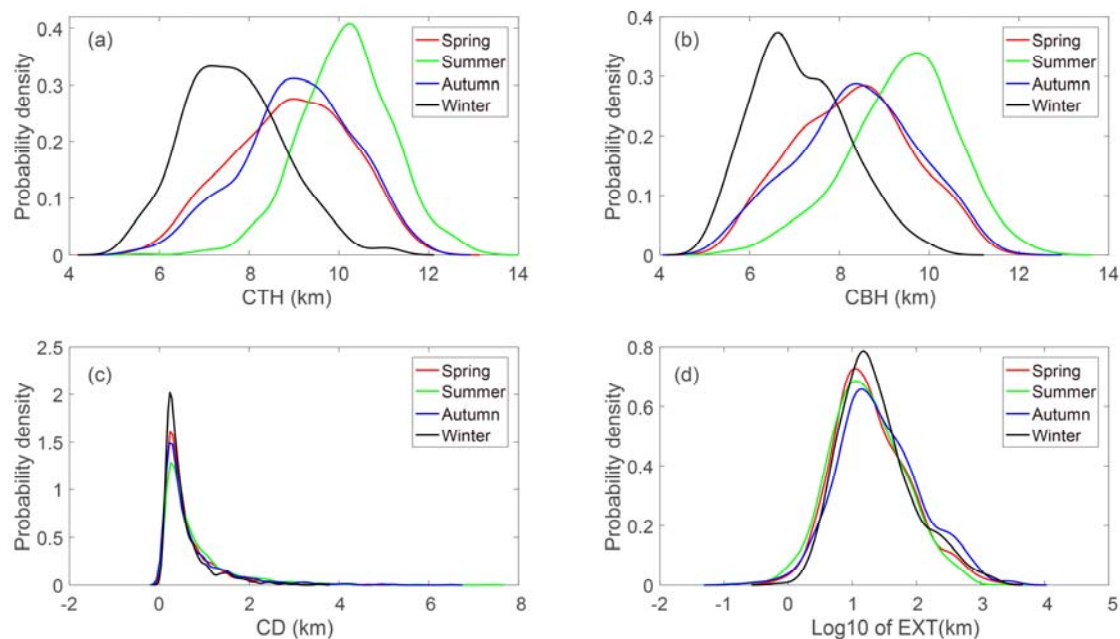
Figure 3. Distribution of cloud-top height (CTH) (a), cloud-base height (CBH) (b), cloud depth (CD) (c) and horizontal extent (EXT) (d) in the four seasons. In (d), EXT is shown as log10 values.

Figure 3b shows that the CBH changes within a range of 5–11.8 km, and the minimum CBHs in the four seasons are close to each other, ranging between 5.0 and 5.5 km. However, the mean CBH in summer is the highest (9.39 km) among the four seasons, while the lowest (7.1 km) is in winter. The difference in CBH between summer and winter is 2.2 km. The CBHs in spring and autumn are 8.30 km and 8.39 km, respectively. In summer, the percentage of cirrus clouds with a CBH larger than 8 km is 87%, while it is only 21% in winter. In winter, 86% of cirrus clouds have a CBH greater than 6 km. The CBH of cirrus clouds in Beijing, especially in winter, is somewhat lower than that reported by Heymsfield et al. (2017), who stated cirrus clouds were generally above 8 km.

It is shown that the mean cloud depths (CDs) of cirrus clouds in the four seasons are close, with the depths of most clusters being less than 1 km (Fig. 3c). Statistically, in the four seasons, 57% of clusters have a CD of less than 0.5 km, 80% less than 1 km, 90% less than 1.5 km, and 95% less than 2km. It is found that the maximum CD is 7.4 km, which occurs in the summer. However, the maximum CD in winter is 3.6 km, which is almost half of that in the summer. It should be noted that the CTH, CBH and CD here are the mean values of a cirrus cluster. It is therefore possible that there are some instances of CTH, CBH and CD that are greater than their corresponding mean values.

The horizontal extent (EXT) of cirrus clouds indicates its lifetime and the formation mechanism type. For the KPDR, the EXT of a cirrus cluster is computed as follows:

$$EXT = V_{hw} \times T_{ci}, \qquad (3)$$

Atmospheric
Chemistry
and Physics

Discussions

Open Access

EGU

where V_{hw} is the mean velocity of horizontal wind calculated from the ECMWF-ERA5 dataset and T_{ci} is the continuous time during which a cirrus cluster moves over the KPDR. It is found that the maximum EXT of cirrus clouds reaches 3100 km, which is in October 2017, and the maximum T_{ci} is 21 hours, which is in March 2016. The EXT ranges through orders of magnitude from low values of less than 0.1 km to over 3000 km. Summer has the minimum mean, median and trimmed mean EXT, while cirrus clouds in autumn have the maximum mean, median and trimmed mean EXT. Statistically, about 75% of cirrus clouds have an EXT less than 50 km and 87% less than 100 km. The statistically quantified structural properties of cirrus clouds in the four seasons are presented in Table 1.

Table 1. Statistical results for the cloud-top height (CTH), cloud-base height (CBH), cloud depth (CD) and horizontal extent (EXT) in the four seasons. The 'trimmean' is the 10% trimmed mean of portion clusters, excluding 10% of clusters with the highest and lowest values (units: km).

| Season	Parameters	Mean	Median	Trimmean	Maximum	Minimum
Spring	CTH	8.95	8.99	8.96	12.18	5.13
	CBH	8.30	8.33	8.295	11.75	5.08
	CD	0.67	0.45	0.58	5.35	0.06
	EXT	60.8	16.6	35.2	2824.9	0.18
	COD	4.43	3.28	3.98	–	0.06
Summer	CTH	10.16	10.18	10.16	13.35	5.49
	CBH	9.39	9.50	9.42	12.83	5.34
	CD	0.77	0.51	0.686	7.4	0.06
	EXT	43.7	15.8	29.7	763.6	0.12
	COD	6.17	4.49	5.76	–	0.1
Autumn	CTH	9.09	9.14	9.12	12.02	5.32
	CBH	8.39	8.42	8.4	11.90	5.11
	CD	0.72	0.43	0.62	6.50	0.06
	EXT	82.2	22.3	51.9	3101	0.10
	COD	4.65	3.14	4.08	–	0.01
Winter	CTH	7.66	7.6	7.64	11.23	5.09
	CBH	7.13	6.97	7.1	10.36	5.01
	CD	0.56	0.38	0.494	3.61	0.07
	EXT	71.9	18.9	40.7	1773.1	0.69
	COD	4.62	2.85	4.14	–	0.26

3.4 Optical depth of cirrus clouds

Cloud optical depths (COD) are relatively independent of wavelength throughout the visible spectrum. In the visible portion of the spectrum, the COD is almost entirely due to scattering by droplets or crystals of clouds (AMS, 2019). Therefore, the

Atmospheric
Chemistry
and Physics
Discussions
Open Access
EGU

205 CODs of cirrus clouds depend directly on the CD, the ice water content, and the size distribution of the ice crystals, indicating a cooling effect or warming effect in the energy budget.

The Advanced Himawari Imager (AHI), onboard the geostationary meteorological Himawari-8 satellite operated by the Japanese Meteorological Agency, observes the Beijing area every 10 min and began releasing COD and cloud-type products in July 2015 with a spatial resolution of 5 km. The CODs are retrieved by using nonabsorbing visible wavelengths (i.e., 0.51

210 or 0.64 μm) and water-absorbing near-infrared wavelengths (i.e., 1.6 or 2.3 μm) (Kawamoto et al. 2001; Nakajima and Nakajma 1995). Quantified uncertainties of the AHI-CODs have not been reported, so we use them here directly. The data nearest to KPDR that both AHI and KPDR determine as cirrus type are selected and their CODs are investigated. Those collocated CODs (collected from the year 2016 to 2017) in the four seasons, combined with the mean CDs and mean reflectivity, which are calculated from KPDR profiles observed within 10 min of the AHI observing time, are presented in

215 Fig. 4.
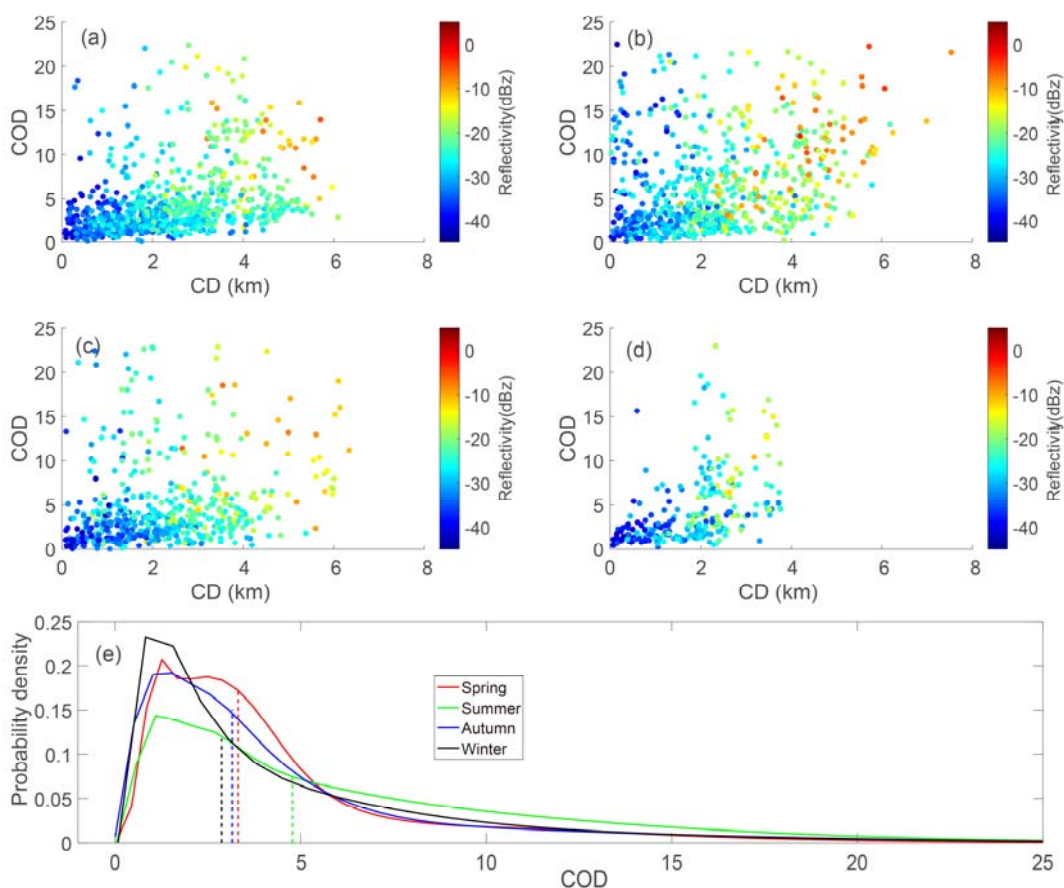
Figure 4. The cloud optical depth (COD) of cirrus clouds in terms of the CD in spring (a), summer (b), autumn (c), and winter (d). Colors indicate the mean radar reflectivity of those radar profiles within 10 min of the AHI observation time. Panel (e) presents the probability density distribution of the COD in the four seasons.

220   In the four seasons, CODs show an increasing tendency with increasing CD. The mean reflectivity shows a similar tendency, meaning thicker cirrus clouds generally contain larger particles and a greater number density of ice particles. The probability density distributions of COD in the four seasons show a higher probability occurring at lower COD. The mean COD in spring, summer, autumn and winter is 4.43, 6.17, 4.65, and 4.62, respectively. The proportions of CODs lower than 3 in spring, summer, autumn and winter are 44%, 35%, 47% and 52%, respectively. The proportions of CODs lower than 10

225   in spring, summer, autumn and winter are 90%, 78%, 87% and 90%, respectively.

4. Microphysical properties of cirrus clouds

The most important microphysical quantities of cirrus clouds are the ice particle size distribution, the ice water content (IWC), and their shapes (Heymsfield et al. 2017). It is known that the radar equivalent (or effective) reflectivity factor (Z_e) can be expressed as

230    $$Z_e = \frac{\lambda^4}{\pi^5} \left| \frac{m^2-1}{m^2+2} \right|^{-2} \iiint \sigma(D,\theta,\Phi) N(D,\theta,\Phi) \mathrm{d}D\mathrm{d}\theta\mathrm{d}\Phi, \quad (4)$$

where $\sigma(D,\theta,\emptyset)$ is the backscattering cross section with maximum dimension D and an axial direction $(\theta,\emptyset)$ with respect to the radar beam, $N(D,\theta,\emptyset)$ is the number density, λ is the wavelength, and m is the complex index of refraction of the scattering target. To date, numerous empirical relationships between Z_e and cloud properties (P)—e.g., IWC, snow precipitation rate—have been developed, usually in the power-law form of

235    $$Z_e = AP^B, \quad (5)$$

where A is the prefactor coefficient and B is the exponent derived in terms of calculated or measured datasets (Austin et al. 2009; Delanoë and Hogan 2010; Deng et al. 2015; Heymsfield et al. 2018; Heymsfield et al. 2008; Liu and Illingworth 2000; Matrosov and Heymsfield 2017; Wang and Sassen 2001a). Delanoë and Hogan (2008, 2010) proposed a different method using a forward model to retrieve the IWC and the effective radius by combination with the COD. Also, the basic principles

240   of this method are applied in the CloudSat/CALIPSO cloud microphysical retrieval algorithm. However, the utility of empirical relations such as Eq. (5) is still common in many practical measurements, and the correspondence between the IWC and Z_e is related with the particle size distribution (the gamma distribution is mostly used for ice clouds).

For the KPDR, the development of the IWC and particle size retrieval algorithm is in progress but has not been tested completely. In this paper, we use the measured radar reflectivity factor Z_e (hereinafter just reflectivity; units: mm^6/m^3;

245   dBZ=10log(Z_e)) directly, not the retrieved microphysical quantities, to study and characterize the microphysical properties of cirrus clouds. It can be found from the Eq. (4) that reflectivity increases when σ and N increase; in other words, a larger reflectivity normally indicates a larger D, N and IWC.


4.1 Reflectivity of cirrus clouds and height dependence

KPDR detects clouds at a 30-m vertical resolution. All cirrus radar bins collected from 2014 to 2017 were counted according

250   to their reflectivity and height, and the relative frequencies are shown separately in Fig. 5. In summer, the reflectivity mostly

varies between −30 and −10 dBZ, while most of the reflectivity falls within the range of −35 to −25 dBZ in winter. In spring and autumn, the reflectivity primarily ranges between −30 and −20 dBZ. The range of variation in reflectivity in summer is the biggest among the four seasons, while it is smallest in winter. Statistically, at the same height where cirrus clouds exist in the four seasons, the mean reflectivity of winter is 5 dBZ less than that of spring or autumn, and it is 10 dBZ less than that of summer. In the four seasons, the mean reflectivity declines as the height increases, with a similar slope. It can also be seen that the cirrus bins in summer are located at higher heights than in winter.
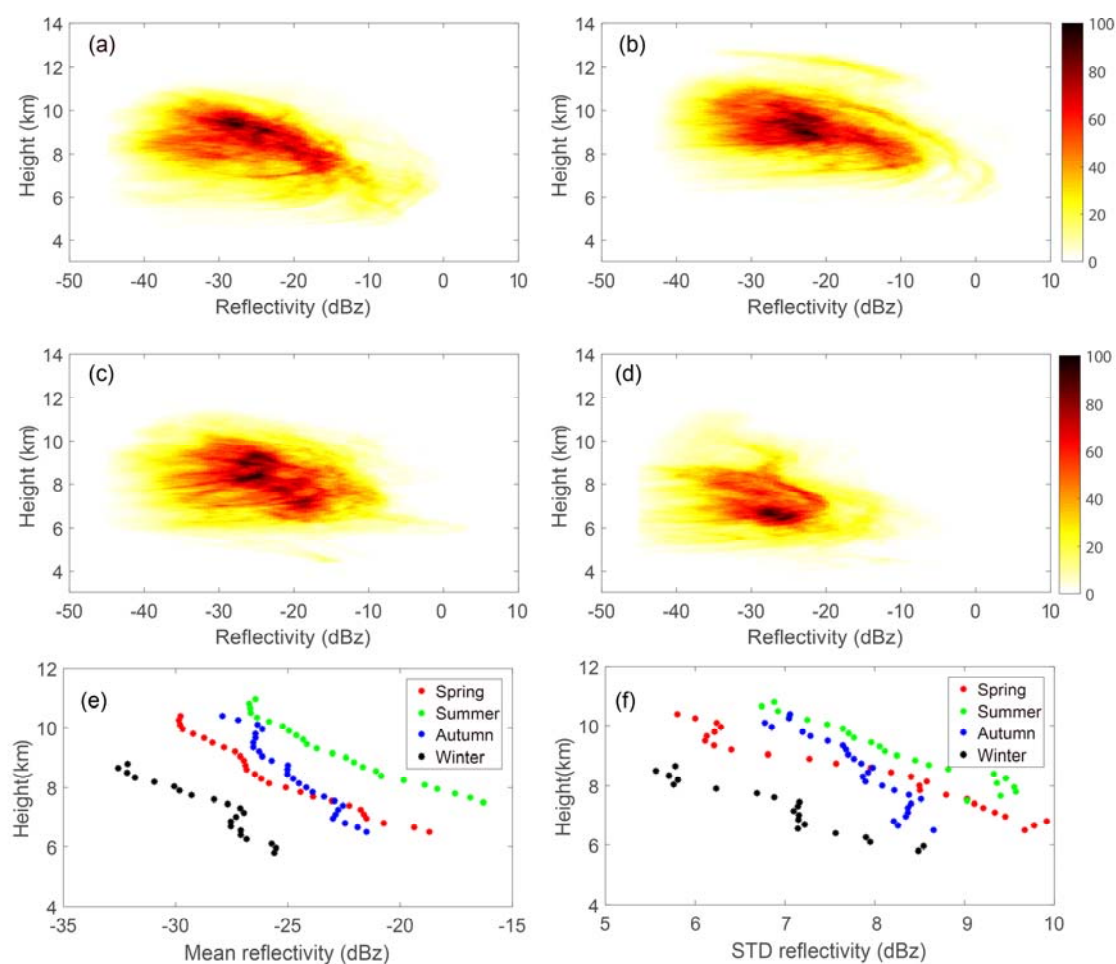

Figure 5. The frequency of reflectivity versus height in spring (a), summer (b), autumn (c) and winter (d). Colors are the values of the numbers divided by 60. The mean reflectivity calculated at various heights and the corresponding standard deviation (STD) are presented in (e) and (f), respectively.

4.2 Temperature dependence

Temperature plays a key role in the formation, evolution and lifetime of cirrus clouds. Activation of liquid waterdrops does not happen below −38ºC because the relative humidity where the ice forms is below water saturation. At temperatures higher than −38ºC, cirrus clouds can form heterogeneously or homogeneously (Kanji et al. 2017). The summer monsoon and winter monsoon in Beijing support distinct temperatures, water vapor, etc., i.e., the conditions necessary for the formation of cirrus clouds, resulting in distributions of reflectivity with different features corresponding to temperature (see Fig. 6).
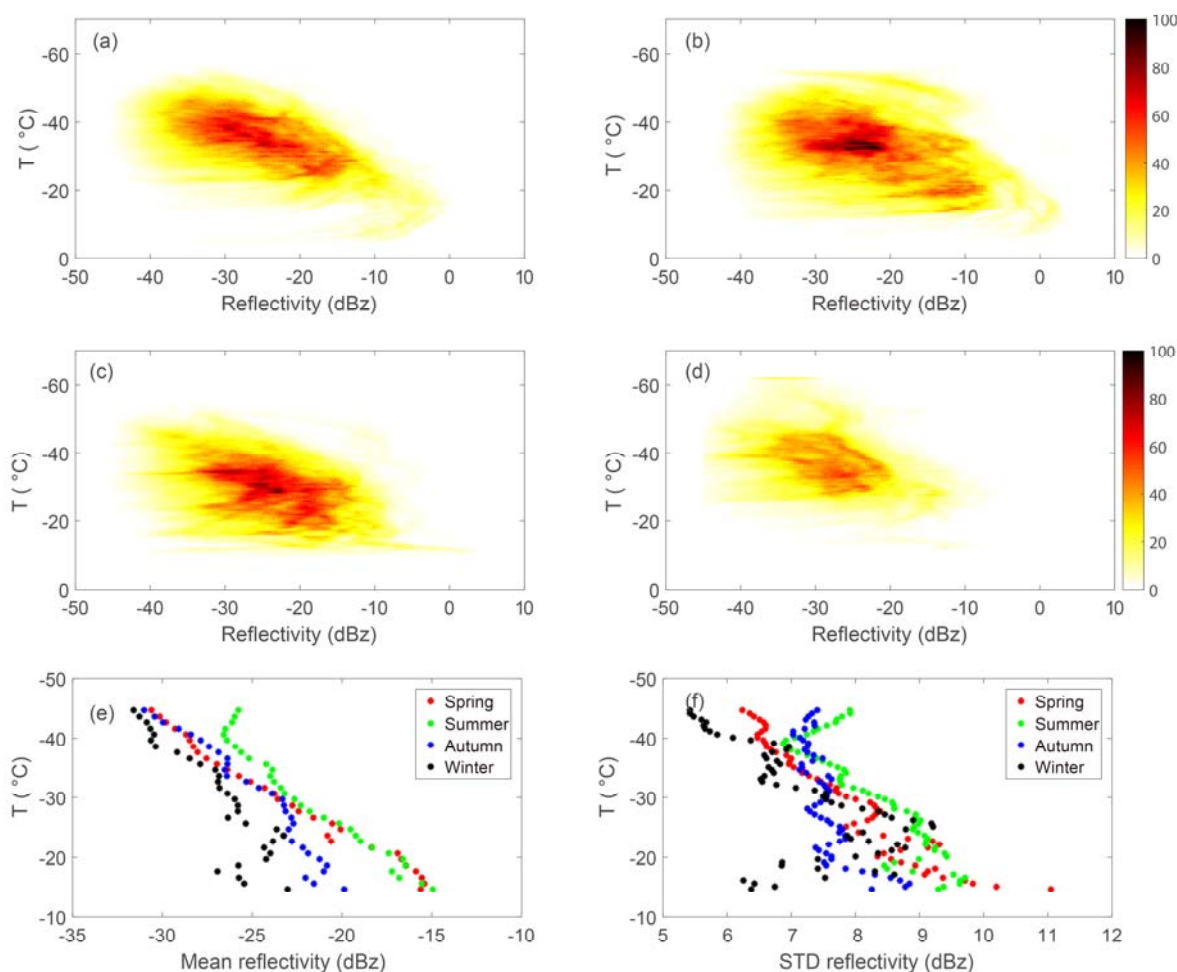
Figure 6. As in Fig. 5 but for temperature, and the colors are the values of the numbers divided by 100.

In spring, summer and autumn, cirrus clouds occur mostly at temperatures within the range of −15ºC to −55ºC, relative to which cirrus clouds in winter occur at lower temperatures. Statistically, the frequency of cirrus bins with temperatures less than −15ºC is 96%, 94%, 95% and 95% in spring, summer, autumn and winter, respectively; the frequency of cirrus bins with temperatures less than −25ºC is 81%, 72%, 66% and 92% in spring, summer, autumn and winter, respectively; the

13

Atmospheric
Chemistry
and Physics
Discussions
Open Access
EGU

frequency of cirrus bins with temperatures less than −35ºC is 45%, 37%, 27% and 55% in spring, summer, autumn and

winter, respectively. The reflectivity shows a dependence on the temperature, increasing when temperature increases.

275 Statistically, the mean temperature of cirrus clouds in winter is lower than that in other seasons, even though these cirrus

clouds appear at lower heights. As the temperature decreases, the difference in reflectivity between winter and summer

declines. At the same temperature, the mean reflectivity in summer is higher than that in winter.

4.3 Depth dependence

Based on all the cirrus clusters in the four years, we calculated the mean reflectivity and the mean depth of each cluster (Fig.

280 7), and it was interesting to find that there is a strong linear relationship between the mean reflectivity and the CD. The mean

reflectivity increases as the CD increases. The linear equation shown in Fig. 7 represents a method that can be used to

estimate the mean reflectivity (or CD) if the CD (or reflectivity) is known, which should be useful for cloud parameterization

in GCMs.
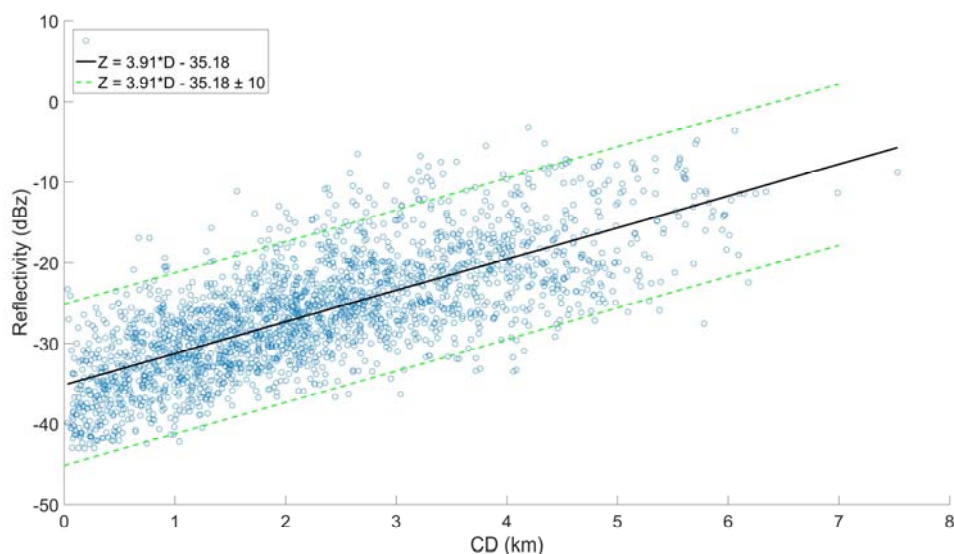
285 **Figure 7.** The mean reflectivity of each cirrus cluster as a function of cloud depth (CD).

5. Origination type of cirrus clouds

Various prefactor coefficients dependent on temperature have been derived and applied in the Z_e–IWC power-law

relationship [i.e., Eq. (5)] since the distribution of reflectivity has a dependence on temperature (Heymsfield et al. 2018;

Heymsfield et al. 2013; Hogan et al. 2006; Matrosov and Heymsfield 2017). Based on the frequency statistics in section 4.2,

290 we also investigated the distribution of reflectivity (similar to the probability density function, PDF) at several temperatures.

Figure 8 shows the normalized frequency of reflectivity at several temperatures (−45ºC, −40ºC, −35ºC, −30ºC, −25ºC,

−20ºC), which are actually portions of Fig. 6. In Fig. 8, we use wider lines to illustrate the data in winter and summer for

clearer contrast since the cirrus clouds show distinct features in the two seasons. Reflectivity's dependence on temperature is also shown in Fig. 8, and the six panels present different distributions of reflectivity at different temperature. Besides, in five

295   of the panels (a, b, c, d, e) of Fig. 8, the frequencies of reflectivity show very close appearances between the summer and winter when reflectivity is lower than −25 dBZ. However, when reflectivity is above −25 dBZ, its PDF in winter declines quickly, illustrating a different appearance with that in summer. The PDFs in winter differ somewhat with those in summer, even at the same temperatures, which may be due to the different origination mechanism of cirrus clouds in the two seasons.
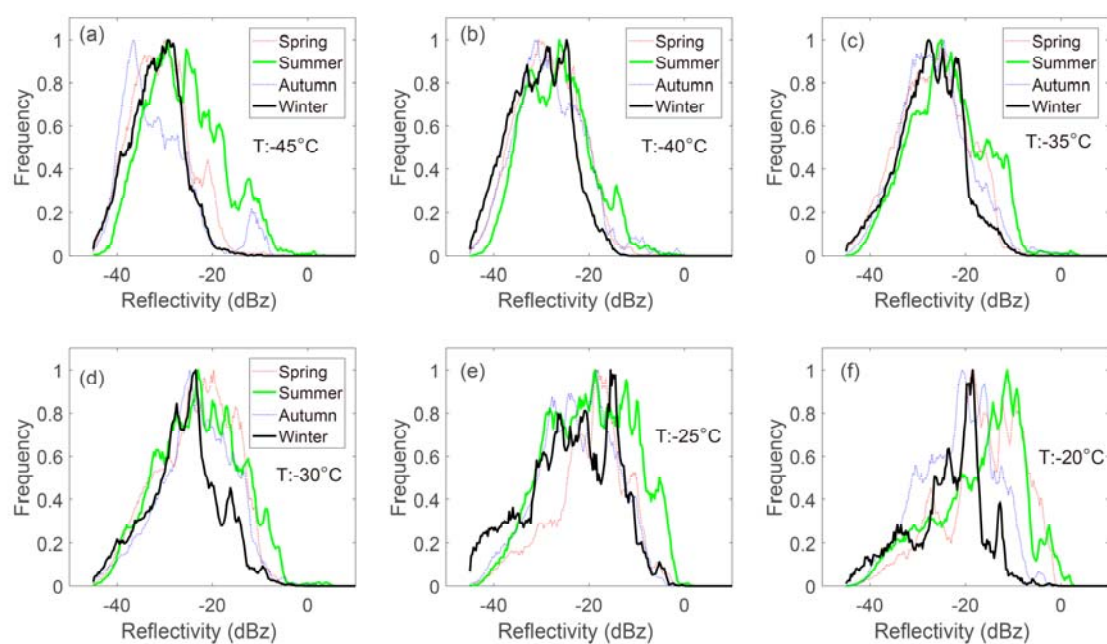
Figure 8. Normalized frequency of the reflectivity at different temperatures in the four seasons. The data from winter (black) and summer (green) are shown with solid and thicker lines for clearer contrast.

        Kramer et al (2016) and Luebke et al. (2016) classified two types of cirrus according to their formation mechanism; namely, *in situ*- and liquid-origin cirrus. The *in situ*-origin cirrus type forms directly as ice, while the liquid-origin type

305   originates from mixed-phase clouds that are completely frozen until they are lifted to the cirrus formation temperature region. They reported that the *in situ*-origin cirrus are mostly thin, with lower IWC, while liquid-origin cirrus tend to be thicker with higher IWC. Also, liquid-origin cirrus tend to have larger ice crystals than *in situ*-origin cirrus. Therefore, the reflectivity of *in situ*-origin cirrus should generally be less than that of liquid-origin cirrus. From the statistical results in Fig. 8, especially panels (a) to (d), it also seems that cirrus clouds in winter below the temperature of −30°C are likely to be *in situ*-origin

310   cirrus, whereas those in summer are formed from both types since the distribution in summer expands to a wider range and

larger reflectivity. Thus, in summer, cirrus with lower reflectivity may be the *in situ*-origin type, while those with higher reflectivity may be the liquid-origin type.

To further test the assumption, we divided the cirrus clusters in summer into two types based on a threshold of mean reflectivity: larger than −30 dBZ (accounting for 30% of all cirrus clusters) and less than −30 dBZ. The mean reflectivity of a
315 cirrus cluster is the mean of the reflectivity of all cirrus bins in the cirrus cluster. We calculated the frequency of cirrus clouds with a mean reflectivity larger than −30 dBZ, which is presented with dashed blue lines in Fig. 9 for comparison. The remaining frequency portions in each panel are from the cirrus clusters with mean reflectivity lower than −30 dBZ.
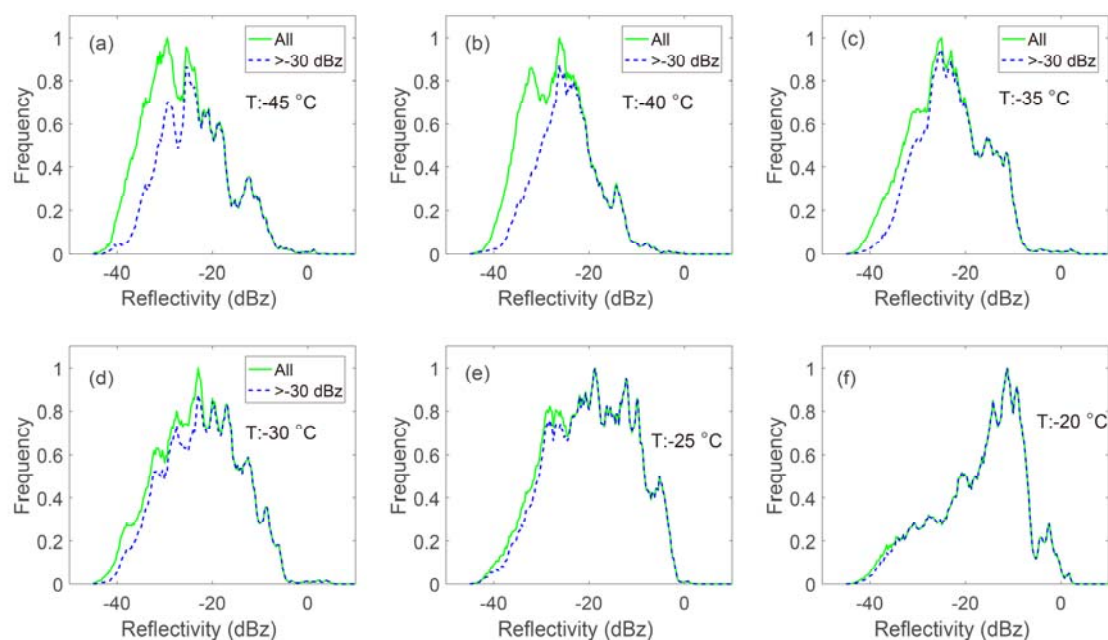
Figure 9. Normalized frequency of the reflectivity at different temperatures of cirrus clouds in summer. The green lines are
320 the same as in Fig.8; the blue dashed lines are calculated based on the cirrus clusters with mean reflectivity larger than −30 dBZ.

When compared with the frequency distribution based on all summer cirrus clusters, these cirrus clusters with mean reflectivity larger than −30 dBZ contribute the absolute majority of those cirrus bins (in Fig. 8) with reflectivity larger than −25 dBZ, illustrating different PDFs with those in winter. Specifically, the differences in the PDFs between winter and
325 summer are mostly due to the cirrus clusters with mean reflectivity higher than −30 dBZ. In particular, as shown in Fig. 9f, those cirrus bins in Fig. 8 are wholly from these clusters with reflectivity larger than −30 dBZ. The strong contrast in Fig. 8f further confirms that the differences in the PDF between summer and winter are due to the different origination type.

From panels (a) to (f) in Fig. 9, as temperature increases, so too does the ratio of those clusters with reflectivity larger than −30 dBZ to all clusters. When the cloud temperature is lower than −30℃, it can be inferred that the cirrus clouds in

330   summer with mean reflectivity lower than −30 dBZ are likely to be of the *in situ*-origin type, while those with mean reflectivity larger than −30 dBZ are likely to be of the liquid-origin type. When cirrus clouds occur at temperatures higher than −30ºC, most will be of the liquid-origin type. In winter, most cirrus clouds are of the *in situ*-origin type. Therefore, the distribution of reflectivity depends not only on the temperature but also on the origin type.

6. Summary and discussion

335   Cirrus clouds are an important component of the planetary radiation budget and remain an uncertainty source in GCMs. This study used four years of vertically pointing Ka-band radar measurements at Beijing to characterize the physical and optical properties of cirrus clouds and to investigate their origination type. The goal was to present the quantified properties of cirrus clouds over the subtropical monsoon zone, which can be represented in GCMs towards a better understanding of the

340   relationships between temperature and radar reflectivity under different formation conditions in various monsoon climates.

Winter monsoon and summer monsoon prevail alternately over Beijing, resulting in four distinct seasons. Cirrus clouds in winter and summer show strikingly different features. The specific findings about the properties of cirrus can be summarized as follows:

1.   The occurrence frequency, height, temperature and mean reflectivity of cirrus in winter are lower than in summer. The

345   average occurrence frequency over Beijing is 16%, and it is 20% in summer but less than 10% in winter. The diurnal variation of the occurrence frequency is not obvious, indicating an insensitive response to solar heating.

2.   The CTHs of cirrus clouds range within 5.09–13.35 km, and the difference between the maximum and minimum reaches 7 km in every season. The mean CTH in summer is 2.5 km higher than in winter. The CBHs range within 5–11.8 km, and the difference in the mean CBH between summer and winter is 2.2 km. In total, 87% of cirrus are above 8 km in summer,

350   and 86% are above 6 km in winter. Statistically, in the four seasons, 57% of clusters have a depth of less than 0.5 km, 80% less than 1 km, and 90% less than 1.5 km.

3.   The EXT ranges through orders of magnitude from low values of less than 0.1 km to over 3000 km. Summer has the minimum mean, median and trimmed mean EXT, whereas cirrus clouds in autumn have the maximum mean, median and trimmed mean EXT. Statistically, about 75% of cirrus clouds have an EXT less than 50 km and 87% less than 100

355   km. In addition, the mean COD in spring, summer, autumn and winter is 4.43, 6.17, 4.65 and 4.62, respectively.

4.   The radar reflectivity of cirrus clouds are dependent on the height, temperature and CD. The reflectivity mostly varies between −35 and −10 dBZ, and the mean reflectivity in summer is 10 dBZ higher than in winter. More than 90% of cirrus bins are below the temperature of −15ºC, and the mean temperature of cirrus in winter is the lowest among the four seasons. It was found that there is a strong linear relationship between the mean reflectivity and the CD.

360   The PDFs of reflectivity with respect to various temperatures were also investigated. It was found that in winter they show an agreement with those in summer when the reflectivity is relatively low; however, when reflectivity gets higher, the

PDFs in winter illustrate striking differences with those in summer. A raw analysis indicated that most cirrus clouds are of the *in situ*-origin type in winter; and when the cloud temperature is lower than −30ºC, cirrus clouds in summer with mean reflectivity lower than −30 dBZ are likely to be of the *in situ*-origin type. In addition, in future work, we intend to further
365 investigate the formation mechanisms of cirrus clouds in Beijing, as well as in other areas, for the purposes of parameterization in GCMs and the development of a locally adaptive Z_e–IWC relationship.

Data Availability

The MODIS product data were obtained from http://ladsweb.nascom.nasa.gov. The AHI data were obtained from https://www.eorc.jaxa.jp/ptree/index.html. The radar data used here are available by special request to the corresponding
370 author (huojuan@mail.iap.ac.cn).

Author contributions

Juan Huo designed the study and carried it out. Yufang Tian, Congzheng Han, Xue Wu, Yinan Wang, Yongheng Bi and Bo Liu prepared some of the datasets. Juan Huo prepared the manuscript with contributions from all co-authors.

Competing interests

375 The authors declare that they have no conflicts of interest.

Acknowledgments

References

Adhikari, L., Z. Wang and M. Deng: Seasonal variations of antarctic clouds observed by cloudsat and calipso satellites. J. Geophys. Res. Atmos., 117(doi:10.1029/2011JD016719), D04202, 2012.

American Meteorological Society, cited 2019: Cirrus. Glossary of Meteorology. Available online at
385 http://glossary.ametsoc.org/wiki/ Cirrus.

Austin, R. T., A. J. Heymsfield and G. L. Stephens: Retrieval of ice and cloud microphysical parameters using the cloudsat millimeter-wave radar and temperature. J. Geophys. Res. Atmos., 114 doi: 10.1029/2008JD010049,2009.

Boucher, O., D. Randall, P. Artaxo, C. Bretherton and e. al: Clouds and aerosols, in climate change 2013: The physical
science basis. Contribution of working group i to the fifth assessment report of the intergovernmental panel on climate
390   change, edited by t. F. Stocker et al.,. Cambridge Univ. Press,Cambridge, U. K., and New York, 2013.

Cotton, R. J., P. R. Field, Z. Ulanowski, P. H. Kaye, E. Hirst, R. S. Greenaway, I. Crawford, J. Crosier and J. Dorsey: The
effective density of small ice particles obtained from in situ aircraft observations of mid-latitude cirrus. Quarterly Journal
of the Royal Meteorological Society, 139(676), 1923-1934, doi: 10.1002/qj.2058,2013.

Delanoë, J. and R. J. Hogan: A variational scheme for retrieving ice cloud properties from combined radar, lidar, and infrared
395   radiometer. J. Geophys. Res. Atmos., 113(D7), doi: 10.1029/2007jd009000,2008.

Delanoë, J. and R. J. Hogan: Combined cloudsat-calipso-modis retrievals of the properties of ice clouds. J. Geophys. Res.
Atmos., 115(D4), doi: 10.1029/2009jd012346,2010.

Deng, M., G. G. Mace, Z. Wang and E. Berry: Cloudsat 2c-ice product update with a new ze parameterization in lidar-only
region. J. Geophys. Res. Atmos., 120(23), 12,198-112,208, doi: 10.1002/2015jd023600,2015.

400   Ge, J., Z. Wang, Y. Liu, J. Su, C. Wang and Z. Dong: Linkages between mid-latitude cirrus cloud properties and large-scale
meteorology at the sacol site. Climate Dynamics, 53 5035–5046, doi: https://doi.org/10.1007/s00382-019-04843-9,2019.

Hahn, C. J. and S. G. Warren (2007). A gridded climatology of clouds over land (1971–96) and ocean (1954–97) from
surface observations worldwide. Numeric Data Product NDP-026E, Carbon Dioxide Information Analysis Center, Oak
Ridge National Laboratory, Oak Ridge.

405   Heymsfield, A., A. Bansemer, N. B. Wood, G. Liu, S. Tanelli, O. O. Sy, M. Poellot and C. Liu: Toward improving ice water
content and snow-rate retrievals from radars. Part ii: Results from three wavelength radar–collocated in situ
measurements and cloudsat–gpm–trmm radar data. J. Appl. Meteorol. Climatol., 57(2), 365-389, doi:
10.1175/jamc-d-17-0164.1,2018.

Heymsfield, A., C. Schmitt and A. Bansemer: Ice cloud particle size distributions and pressure-dependent terminal velocities
410   from in situ observations at temperatures from 0° to 86°c. J. Atmos. Sci., 70 4123–4154, doi:
doi:10.1175/JAS-D-12-0124.1,2013.

Heymsfield, A. J., M. Krämer, A. Luebke, P. Brown, D. J. Cziczo, C. Franklin, P. Lawson, U. Lohmann, G. McFarquhar, Z.
Ulanowski and K. V. Tricht: Cirrus clouds. Meteorological Monographs, 58 2.1-2.26, doi:
10.1175/amsmonographs-d-16-0010.1,2017.

415   Heymsfield, A. J., A. Protat, D. Bouniol, R. T. Austin, R. J. Hogan, J. Delanoë, H. Okamoto, K. Sato, G.-J. v. Zadelhoff, D. P.
Donovan and Z. Wang: Testing iwc retrieval methods using radar and ancillary measurements with in situ data. J. Appl.
Meteorol. Climatol., 47(1), 135-163, doi: 10.1175/2007jamc1606.1,2008.

Hogan, R. J., M. P. Mittermaier and A. J. Illingworth: The retrieval of ice water content from radar reflectivity factor and
temperature and its use in evaluating a mesoscale model. J. Appl. Meteorol. Climatol., 45(2), 301-317, doi:
420   10.1175/jam2340.1,2006.

Huo, J., Y. BI, D. Lu and S. Duan: Cloud classification and distribution of cloud types in beijing using ka band radar data.

Atmospheric
Chemistry
and Physics
Discussions

Advances in Atmospheric Sciences, 36 1-11, doi: https://doi.org/10.1007/s00376-019-8272-1.,2019.

Jensen, E. J., O. B. Toon, H. B. Selkirk, J. D. Spinhirne and M. R. Schoeberl: On the formation and persistence of subvisible cirrus clouds near the tropical tropopause. J. Geophys. Res. Atmos., 101(D16), 21361-21375, doi:

425   10.1029/95jd03575,1996.

Joos, H., P. Spichtinger, P. Reutter and F. Fusina: Influence of heterogeneous freezing on the microphysical and radiative properties of orographic cirrus clouds. Atmos. Chem. Phys.,, 6835–6852, doi: doi:10.5194/acp-14-6835-2014,2014.

Kanji, Z. A., L. A. Ladino, H. Wex, Y. Boose, M. Burkert-Kohn, D. J. Cziczo and M. Krämer: Overview of ice nucleating particles. Meteorological Monographs, 58 1.1-1.33, doi: 10.1175/amsmonographs-d-16-0006.1,2017.

430   Kärcher, B.: Formation and radiative forcing of contrail cirrus. Nature Communications, 9(1), 1824, doi: 10.1038/s41467-018-04068-0,2018.

Kawamoto, K., T. Nakajima and T. Y. Nakajima: A global determination of cloud microphysics with avhrr remote sensing. Journal of Climate, 14(9), 2054-2068, doi: 10.1175/1520-0442(2001)014<2054:Agdocm>2.0.Co;2,2001.

Kollias, P., E. E. Clothiaux, M. A. Miller, B. A. Albrecht, G. L. Stephens and T. P. Ackerman: Millimeter-wavelength radars:

435   New frontier in atmospheric cloud and precipitation research. Bulletin of the American Meteorological Society, 88(10), 1608-1624, doi: 10.1175/bams-88-10-1608,2007.

Kox, S., L. Bugliaro and A. Ostler: Retrieval of cirrus cloud optical thickness and top altitude from geostationary remote sensing. Atmos. Meas. Tech., 7(10), 3233-3246, doi: 10.5194/amt-7-3233-2014,2014.

Krämer, M., C. Rolf, A. Luebke, A. Afchine, N. Spelten, A. Costa, J. Meyer, M. Zöger, J. Smith, R. L. Herman, B. Buchholz,

440   V. Ebert, D. Baumgardner, S. Borrmann, M. Klingebiel and L. Avallone: A microphysics guide to cirrus clouds – part 1: Cirrus types. Atmos. Chem. Phys.,, 16 3463–3483,, doi: doi:10.5194/acp-16-3463-2016,2016.

Lawson, R. P., S. Woods, E. Jensen, E. Erfani, C. Gurganus, M. Gallagher, P. Connolly, J. Whiteway, A. J. Baran, P. May, A. Heymsfield, C. G. Schmitt, G. McFarquhar, J. Um, A. Protat, M. Bailey, S. Lance, A. Muehlbauer, J. Stith, A. Korolev, O. B. Toon and M. Krämer: A review of ice particle shapes in cirrus formed in situ and in anvils. J. Geophys. Res. Atmos.,

445   124 10049–10090, doi: https://doi.org/10.1029/2018JD030122,2019.

Liu, C.-L. and A. J. Illingworth: Toward more accurate retrievals of ice water content from radar measurements of clouds. Journal of Applied Meteorology, 39(7), 1130-1146, doi: 10.1175/1520-0450(2000)039<1130:Tmaroi>2.0.Co;2,2000.

Luebke, A. E., A. Afchine, A. Costa, J. U. Grooß, J. Meyer, C. Rolf, N. Spelten, L. M. Avallone, D. Baumgardner and M. Krämer: The origin of midlatitude ice clouds and the resulting influence on their microphysical properties. Atmos. Chem.

450   Phys., 16(9), 5793-5809, doi: 10.5194/acp-16-5793-2016,2016.

Mace, G., S. Benson and E. Vernon: Cirrus clouds and the large-scale atmospheric state: Relationships revealed by six years of ground-based data. J. Climate Appl. Meteor., 19 3257-3278, doi: doi:10.1175/JCLI3786.1,2006.

Matrosov, S. Y. and A. J. Heymsfield: Empirical relations between size parameters of ice hydrometeor populations and radar reflectivity. J. Appl. Meteorol. Climatol., 56(9), 2479-2488, doi: 10.1175/jamc-d-17-0076.1,2017.

455   Muhlbauer, A., T. P. Ackerman, J. M. Comstock, G. S. Diskin, S. M. Evans, R. P. Lawson and R. T. Marchand: Impact of

large-scale dynamics on the microphysical properties of midlatitude cirrus. J. Geophys. Res. Atmos., 119 3976–3996, doi: doi:10.1002/2013JD020035,2014.

Nakajima, T. Y. and T. Nakajma: Wide-area determination of cloud microphysical properties from noaa avhrr measurements for fire and astex regions. Journal of the Atmospheric Sciences, 52(23), 4043-4059, doi:

460   10.1175/1520-0469(1995)052<4043:Wadocm>2.0.Co;2,1995.

Sassen, K., Z. Wang and D. Liu: Global distribution of cirrus clouds from cloudsat/cloud-aerosol lidar and infrared pathfinder satellite observations (calipso) measurements. J. Geophys. Res., 113(D00A12), doi: doi:10.1029/2008JD009972,2008.

Sassen, K., Z. Wang and D. Liu: Cirrus clouds and deep convection in the tropics: Insights from calipso and cloudsat. J.

465   Geophys. Res. Atmos., 114 doi: D00H06, doi:10.1029/2009JD011916,2009.

Stubenrauch, C. J., A. Chedin, G. Radel, N. A. Scott and S. Serrar: Cloud properties and their seasonal and diurnal variability from tovs path-b. J. Clim., 19(21), 5531–5553, 2006.

Wang, Z. and K. Sassen: Cirrus cloud microphysical property retrieval using lidar and radar measurements. Part i: Algorithm description and comparison with in situ data. Journal of Applied Meteorology, 41 218-229, 2001a.

470   Wang, Z. and K. Sassen: Cloud type and macrophysical property retrieval using multiple remote sensors. Journal of Applied Meteorology, 40(10), 1665-1682, doi: 10.1175/1520-0450(2001)040<1665:Ctampr>2.0.Co;2,2001b.

Wolf, V., T. Kuhn, M. Milz, P. Voelger, M. Krämer and C. Rolf: Arctic ice clouds over northern sweden: Microphysical properties studied with the balloon-borne ice cloud particle imager b-ici. Atmos. Chem. Phys., 18(23), 17371-17386, doi: 10.5194/acp-18-17371-2018,2018.

475   Yang, P., K. N. Liou, L. Bi, C. Liu, B. Yi and B. A. Baum: On the radiative properties of ice clouds: Light scattering, remote sensing, and radiation parameterization. Adv. Atmos. Sci.,, 32 doi: https://doi.org/10.1007/s00376-014-0011-z,2015.

Yang, P. and Q. Fu: Dependence of ice crystal optical properties on particle aspect ratio. Journal of Quantitative Spectroscopy and Radiative Transfer, 110(14–16), 1604-1614, doi: https://doi.org/10.1016/j.jqsrt.2009.03.004,2009.

Zelinka, M. D., S. A. Klein and D. L. Hartmann: Computing and partitioning cloud feedbacks using cloud property

480   histograms. Part i: Cloud radiative kernels. J. Clim., 25(11), 3715–3735, 2012.